bioRxiv preprint doi: https://doi.org/10.1101/2021.03.07.434162; this version posted March 8, 2021. The copyright holder for this preprint (which was not certified by peer review) is the author/funder. All rights reserved. No reuse allowed without permission.

Structured Modulations of Ongoing Variability by Task and Development

Shruti Naik[1], Parvaneh Adibpour[1], Jessica Dubois[1,2], Ghislaine Dehaene-Lambertz[1]*, Demian Battaglia[3,4]*

[1] Cognitive Neuroimaging Unit U992, NeuroSpin Center, F-91190 Gif/Yvette, France.

[2] Université de Paris, NeuroDiderot, Inserm, F-75019 Paris, France.

[3] Institute for Systems Neuroscience U1106, Aix-Marseille Université, F-13005 Marseille, France.

[4]University of Strasbourg Institute for Advanced Studies (USIAS), F-67000 Strasbourg, France.

* Shared lead and corresponding authorship: Demian Battaglia and Ghislaine Dehaene-Lambertz

Email: demian.battaglia@univ-amu.fr and ghislaine.dehaene-lambertz@cea.fr

ORCID Demian Battaglia: 0000-0003-2021-7920

ORCID Ghislaine Dehaene-Lambertz: 0000-0003-2221-9081

bioRxiv preprint doi: https://doi.org/10.1101/2021.03.07.434162; this version posted March 8, 2021. The copyright holder for this preprint (which was not certified by peer review) is the author/funder. All rights reserved. No reuse allowed without permission.

SUMMARY

Patterns of trial-averaged post-stimulus neural activity, e.g. event related potentials (ERPs) are traditionally interpreted as the correlates of cognitive operations. However, single-trial trajectories of neural responses approach these ERP components only in a loose and stochastic manner, questioning legitimacy of these components' proposed roles. Deconstructing the conventional ERP analyses, here we studied patterns of event related variability (ERV) in 2-6 month-old infants and adults using electroencephalography. Our analyses reveal that the ERP components are analogous to the biasing forces on the ongoing dynamics, which instrument the variability quenching and boosting events along neural trajectories. Moreover, the observed ERV possesses a rich temporal structure, modulated by both age and task, rivaling in complexity with that of the classical ERPs. Our findings suggest that since the early infancy, neural trajectories are actively controlled. This is compliant with the hypothesis that neural variability is a resource for cognitive processing, rather than unwanted noise.

bioRxiv preprint doi: https://doi.org/10.1101/2021.03.07.434162; this version posted March 8, 2021. The copyright holder for this preprint (which was not certified by peer review) is the author/funder. All rights reserved. No reuse allowed without permission.

INTRODUCTION

Since Wundt (1832-1920), the purpose of experimental and later of cognitive psychology has been to decompose complex brain functions into simpler processes, or mental operations, that could be studied in relative isolation thanks to the careful manipulation of experimental parameters(Posner and DiGirolamo, 2000). Following this ambition, thousands of studies have been published each year in which the peaks and troughs of average, stimulus-locked neural time-series (e.g. ERPs (Event-Related Potentials), as measured with electroencephalography (EEG)) have been explained as neural correlates of cognitive operations. It is indeed quite remarkable that averaging neural signals across multiple presentations of the same stimulus recovers robust and reproducible responses across participants. The ERP literature has progressively identified specific neural components whose latency and scalp-topography signifies particular cognitive operations from sensory processes (e.g. recognition of faces (N170), to high-level processes (e.g. detecting lexicon incongruencies (N400), or monitoring our own behavioral errors (ERN: error related negativity))(Luck, 2012).

In this framework, the ongoing/background activity is considered as an unwanted noise discarded through the averaging process(Jasper, 1937). While some measurement errors and artefacts are indeed unwanted(Verleger, Gasser and Möcks, 1982), the trial-by-trial variation of the recorded signal could also be a genuine property of the participant's brain(Wu *et al.*, 2014). Furthermore, since complete cognitive processes take place within each individual trial, and "mental operations" can vary from one trial to the next (e.g. stimulus visibility at threshold, confidence variation, change of strategy, etc), the signature of these operations should be detectable within individual trials-- without averaging. This methodological tour-de-force is sometimes accomplished by powerful time-series preprocessing or machine learning algorithms(Jung *et al.*, 2001; Vahid *et al.*, 2020). However, all these methods

bioRxiv preprint doi: https://doi.org/10.1101/2021.03.07.434162; this version posted March 8, 2021. The copyright holder for this preprint (which was not certified by peer review) is the author/funder. All rights reserved. No reuse allowed without permission.

implicitly assume that the pertinent ERP is a weak signal sunk in uncorrelated noise. Is this tenet itself as straightforward as it seems?

An increasing number of studies suggest that background activity fluctuations in sensory areas can bias perceptual report and in attention network affect stimulus detection, thus participating in the cognitive process itself and conveying important task-relevant information, crucial for efficient cognitive function(Hesselmann *et al.*, 2008; Sadaghiani, Hesselmann and Kleinschmidt, 2009). Furthermore, post-stimulus activity and ongoing fluctuations do not simply add up but nonlinearly interact(He, 2013) explaining the resulting perception and behavior(VanRullen *et al.*, 2011). Finally, spontaneous and stimulus-related activity share similarities(Kenet *et al.*, 2003) that increase along development, possibly reflecting priors about the structure of the environment which is progressively internally encoded(Berkes *et al.*, 2011).

In such alternative framework, brain activity is thought to unfold along erratic trajectories in the high-dimensional space of possible configurations of a dynamical system, shaped by the exploration of a complex landscape of dynamic attractors(Mazor and Laurent, 2005; Chaudhuri *et al.*, 2019). This activity can then be modulated by task demands, arousal, vigilance, etc. at the moment of stimulus presentation(Huk, Bonnen and He, 2018). Compatible with this scenario, it was indeed observed that inter-trial variability is not constant but is characteristically reduced in the post-stimulus period with respect to baseline at rest. This “variability quenching” after stimulus presentation is a cortex-wide phenomenon robustly observed at many spatiotemporal scales and across many different tasks(Churchland *et al.*, 2010; Arazi, Censor and Dinstein, 2017). It is interpreted as neural trajectories being actively constrained by the task to be more reproducible. In human adults, this quenching is further increased by endogenous biases, such as active attention(Broday-Dvir *et al.*, 2018) or conscious awareness(Schurger *et al.*, 2015).

bioRxiv preprint doi: https://doi.org/10.1101/2021.03.07.434162; this version posted March 8, 2021. The copyright holder for this preprint (which was not certified by peer review) is the author/funder. All rights reserved. No reuse allowed without permission.

Most observed quenching phenomena immediately follows stimulus presentation, and several computational models could explain such mechanistic variability reduction as a byproduct of the stimulus presentation itself(Rajan, Abbott and Sompolinsky, 2010; Litwin-Kumar and Doiron, 2012; Hennequin *et al.*, 2018). The hypothesis that variability modulations are not an epiphenomenon but play active role in information processing and reflect cognitive processing stages needs new evidence, dismissing the possibility of "trivial" quenching.

One of the appealing aspects of classical ERP analyses is the succession of discrete components -- retrievable at various latencies in the time-course of the average stimulus-induced response that can be attached to different cognitive operations. The identification of an analogously rich temporal structure in the dynamics of response variability would both dismiss "trivial" quenching and potentially suggest that variability modulation might also be a usable marker of cognitive steps, similarly to monitoring the spreading of birds in a flock (– a metaphor for different trial trajectories in an ensemble of trials–); which may signal a food source, a predator or the wind direction. Furthermore, the modulation of neural variability might not be limited to quenching. Increased variability might point to a broader repertoire and flexibility of brain states instrumental for task-dependent cognitive processing(McIntosh, Kovacevic and Itier, 2008; Naik *et al.*, 2017).

Hence we searched here for a richly structured dynamics of response variability by reanalyzing high-density EEG data obtained in 5 to 24-week-old human infants(Adibpour, Dubois and Dehaene-Lambertz, 2018) as well as in adults when they were presented with human faces. We chose to study this question in human infants for two reasons: Firstly, because maturation; notably in the visual domain, is intense during the first semester of life(Braddick and Atkinson, 2011). We hypothesized that these changes would have an intricate neural effect on the functional dynamics at this rapidly changing period than during

bioRxiv preprint doi: https://doi.org/10.1101/2021.03.07.434162; this version posted March 8, 2021. The copyright holder for this preprint (which was not certified by peer review) is the author/funder. All rights reserved. No reuse allowed without permission.

the stable adult stage. The second reason is the observation that human infants are exceptional learners(Dehaene-Lambertz and Spelke, 2015). If variability modulation is an intrinsic part of the building and manipulation of internals models(Berkes *et al.*, 2011), the fast learning pace of infanthood might reveal more complex dynamical changes of stimulus relevant variability than the adults who possess relatively stable internal models. Furthermore, it is a common belief that unwanted ongoing activity compromises the robustness and reproducibility of infant ERPs. Given this belief, a better understanding of the potential structure of the variability modulation in single-trial responses might lead to better models of cerebral development and learning and tools to gauge infant cognition.

We considered three indicators to capture the main characteristics of trial-variability (see cartoon representations in Fig. 1E): First we characterized ***ERP flybys****:* given the mere existence of ERP components (corresponding to recognizable group-level scalp topographies at expected time-windows following a stimulus), we sought to quantify how the trajectory of each individual trial approached these topographies. We evaluated in each subject, the distributions of the closest single-trial-distances to the template but also the distributions of the latencies of the closest distance. Secondly, we examined ***between trial variability*** to quantify how close (or far) individual trials trajectories were to each other as they evolved in time. It corresponds to the variability quenching described earlier; thirdly we introduced a suitable metric of the instantaneous rate of brain state reconfiguration –***within-trial variability*** or ***within-trial speed***- to track modulations of trajectory variability along individual trials.

To get a visual sense of these indicators, consider a flock of birds again. Each bird can fly on its own trajectory with its own speed. If some interesting landmark exists (e.g. a utility pole), each bird will eventually “fly by” that location. However, not all birds will approach this landmark exactly at the same time or at the same distance, creating a distribution of

bioRxiv preprint doi: https://doi.org/10.1101/2021.03.07.434162; this version posted March 8, 2021. The copyright holder for this preprint (which was not certified by peer review) is the author/funder. All rights reserved. No reuse allowed without permission.

latencies of individual bird's fly-bys to this landmark but also a distribution of fly-by distances from the landmark. Note that birds can come closer to each other at any given moment, regardless of the reference landmark and also be close to the landmark without being close to each other. Hence, one can measure the "spread of the flock" to understand how far or close these birds remain regardless of where they are with respect to the important landmarks. This is equivalent to measuring between-trial variability at any given time.

Moreover, one could measure the instantaneous motion speed of individual birds in the vicinity of the landmark, in an attempt to uncover the detailed kinematics of approaching the utility pole and then leaving away. Some birds may accelerate getting close to the pole but slowdown in its immediate proximity in order to avoid collision. In the same vein, we quantify with our third indicator the instantaneous rate of fluctuation in single-trial topography evolution, to assess the speed of their reconfiguration and the speed profiles characteristically associated to ERP components flybys.

Indeed, despite the simplicity of the tasks, we observed in our young participants, a surprisingly complex temporal organization of response variability-- induced by the central or lateral face stimuli. This organization gradually emerged through early infancy, and by the second trimester of life, reached to a spatiotemporal structure remarkably similar to the one confirmed in adults. Moreover, these characteristic sequences of variability modulations were dependent on the task at hand. We propose the term *Event-Related Variability* (ERV), to collectively describe this remarkable sequential and task-specific organization of flybys, variability quenching and boosting events, both between and within trials, which rivals in complexity with classic descriptions of the modulations of average response (ERP). Such ERV dynamics was nontrivial and highly organized in both adults and infants, revealing an immediate richness of structured states in infants comparable to later ages. It suggests that ERV could serve as a computing resource in infants.

bioRxiv preprint doi: https://doi.org/10.1101/2021.03.07.434162; this version posted March 8, 2021. The copyright holder for this preprint (which was not certified by peer review) is the author/funder. All rights reserved. No reuse allowed without permission.

RESULTS

1) Event-Related Potentials (ERP) evoked by face presentation in infants and adults

Both infants (N=39, 5-24 weeks) and young adults (N=13, 21-27 years) followed rapid presentation of unfamiliar faces (alternatively between the lateral hemi-fields) and for a subset of infants (N=22, 5-22 weeks), also in the central visual field (Fig 1A(Adibpour, Dubois and Dehaene-Lambertz, 2018)). Classical ERP analyses revealed two prominent ERP components: an early "P1" and a late "P400". These components are commonly identified in infants in response to visual image, have different neural basis and correspond to different cognitive stages(De Haan, Johnson and Halit, 2003). They were clearly visible at the grand average level and had clear equivalent topographies in adults (cf. Fig 1B for infants and Fig S1A for adults). For adults, latencies were faster, voltage topographies qualitatively similar and overall ERP signal amplitude weaker as compared to infants. For lateral faces: the P1 response was evident as the first positivity on the contra-lateral posterior electrodes ~250-300 ms following face onset in infants (Fig 1B) and ~100 ms in adults (Fig S1 A). The P400 response was a large bilateral positivity on occipitotemporal clusters following P1 response around 500-600 ms (~400 ms in adults). For central faces, latencies were faster relative to lateralized faces, around 150 ms for the P1 visible on medial posterior electrodes and around 450-550 ms for the P400 on occipitotemporal channels (Fig 1 B bottom row). The overall signal amplitude was larger for central than for the lateral faces. These results are in agreement with previous literature on ERP dynamics following face presentation in adults and infants(De Haan, Johnson and Halit, 2003; Conte *et al.*, 2020). Infant N290 topography was not prominent and adult N170 topography did not find clear equivalence in infants, hence we avoided these "intermediate" components.

bioRxiv preprint doi: https://doi.org/10.1101/2021.03.07.434162; this version posted March 8, 2021. The copyright holder for this preprint (which was not certified by peer review) is the author/funder. All rights reserved. No reuse allowed without permission.

2) Ongoing Variability Dominates ERP

While characteristic ERPs existed, single-trial responses were noisy and hardly resembled grand averaged responses (Fig 1C; Fig S1B), typically remaining one- or two- order of magnitude larger than ERP amplitudes in both adults and infants, with extremely variable topographies and no clear peaks or valleys corresponding to the ERP. To illustrate the relationship between ongoing and evoked activity, we show in Fig. 1D a 12 s-long-segment of continuous EEG data for a representative infant (age=15.4 weeks). At every time point, brain topography is represented by a 3-dimensional vector (of activity amplitudes after applying Principle Component Analysis, see *methods*). If stimulus presentation always evoked a similar single-trial trajectory, the EEG trajectory time points recorded immediately following the presentation of a face stimulus should cluster together within our low-dimensional projection. Contrarily, post-stimulus trajectory snippets (highlighted in red in Fig. 1D) were distributed nearly uniformly through the sampled space. This dispersion suggests that post-stimulus temporal fluctuations of neural trajectory were predominantly determined by the ongoing activity. In particular, individual stimulus presentation events did not lead to a radical reset of the activation topographies and did not constrain them to strongly resemble the average reference topographies.

With the hypothesis that this tremendous response variability and moment-to-moment fluctuations might carry important information regarding the underlying neural and cognitive processes, we considered three indicators to quantify the signal variability (see cartoon representations in Fig. 1E): *ERP component flybys, between trial variability* and *within-trial variability (or trial Speed)*. We used multivariate pattern dissimilarity with correlation distance (i.e. 1 – Pearson Correlation Coefficient) as a metric of dispersion (see *Methods*). Results from all the three approaches are summarized in the following sections.

bioRxiv preprint doi: https://doi.org/10.1101/2021.03.07.434162; this version posted March 8, 2021. The copyright holder for this preprint (which was not certified by peer review) is the author/funder. All rights reserved. No reuse allowed without permission.

3) Single-trial flybys to classic ERP components are modulated by age and hemisphere

Despite erratic trajectories, grand average ERP topographies are reproducible across studies suggesting they capture stimulus-relevant information. Hence we analyzed how individual trials approach (fly-by) these "landmark events" (i.e., in our bird flock metaphor, how close and when individual birds in the flock approach the pole). We defined the grand averaged P1 and P400 topographies (separately for infants and adults) as "ERP-templates" and examined the distributions of the latencies and distances of the single-trial flybys to these templates (Fig 2 and S3, see *Methods*).

For all task-conditions, trials remained quite far from the ERP-templates most of the time (flyby distance ~0.8- 1; Pearson correlation: 0-0.2, Fig2A, FigS3A, B). However, individual trial trajectories slightly and significantly reduced their distance to the ERP-templates around specific latencies (Distance drops in Fig. 2A and S3A respectively for right and left faces, emphasized by red vertical lines). For lateral faces, trials approached the P1-template around [150, 350] ms; and the P400-template about [400,600] ms post-stimulus onset. For the central faces, closest approach to P1- and P400-templates occurred about [-150, 150] ms and [350, 550] ms respectively (Fig S3 B).

To quantify age-dependency of flyby latencies and latency jitters around the ERP components, we estimated distribution of closest single-trial flybys for each infant and adult, and studied whether their medians and standard deviations were correlated with age.

Fly-by latencies: The median of the flyby latencies to both the P1- and P400-templates significantly decreased with infant's age for the faces presented on the right hemi-field (P1: $r= -0.39$, $p<0.006$ from ~280 ms at 5 weeks to ~200 ms at 24 weeks; P400: $r= -0.38$, $p<0.009$ from ~600 ms to ~500 ms, Fig. 2A) but not for left or central hemi-field (Fig S3 C,D top panels). This initial delay in fly-by latencies for the right faces (processed by the left-hemisphere) in the youngest infants, congruent with several results showing a slower

bioRxiv preprint doi: https://doi.org/10.1101/2021.03.07.434162; this version posted March 8, 2021. The copyright holder for this preprint (which was not certified by peer review) is the author/funder. All rights reserved. No reuse allowed without permission.

maturation of the left hemisphere compared to right(Chiron *et al.*, 1997) suggest a catch-up relatively to the more mature right hemisphere during this period. Median fly-by latencies for adults were much faster than that of infants, continuing thus the decreasing latency trend already observed over the first two semesters of life (inset box-plots in Fig. 2B and Fig S3 C top panel; P1 median latencies across adults: 96 ± 13 ms for right faces and 83 ± 6 ms for left faces; P400 median latencies: 312 ± 20 ms for right faces and 308 ± 18 ms for left faces).

Spread of fly-by latencies: Did age modulate the temporal precision of the fly-bys, i.e. did all the trials approach the ERP-templates precisely at the median time for all babies or did they fluidly pass close to these templates at different times? The standard deviation of the closest flyby latencies varied ~40-60 ms from their respective medians in each infant. Surprisingly, even though infants on an average became faster to approach the ERP-templates, the "spread" of the P1-flyby latencies significantly increased with age (Fig 2B left bottom panel, $r = 0.45$, $p<0.002$), suggesting that the infants became less temporally precise or more flexible in approaching P1-template (loose formation of the flock around this pole). By contrast, the spread of P400-flybys showed a moderate negative trend (Fig 2B, right bottom panel, $r = -0.26$, $p<0.055$), suggesting that infants became more temporally precise in approaching the P400-like state (tighter flock formation around this pole). Again, this effect was significant only for the right faces but not left or central faces (Fig S3 C, D bottom panels), another indication that the left hemisphere was catching up with the right hemisphere in terms of maturation or perhaps indicating the ongoing maturation of corpus-callosum(Adibpour, Dubois and Dehaene-Lambertz, 2018). Interestingly, adults also showed a ~40-60 ms jitter across trials as compared to their median P1 and P400-flyby latencies

bioRxiv preprint doi: https://doi.org/10.1101/2021.03.07.434162; this version posted March 8, 2021. The copyright holder for this preprint (which was not certified by peer review) is the author/funder. All rights reserved. No reuse allowed without permission.

(Figure 2 B box plots: P1-latency jitters: 54 ± 4ms for right and 50 ± 5ms for left faces; P400 latency jitters: 57 ± 3 ms and 56 ± 2 ms for right and left faces respectively).

Mean and dispersion of flyby distances: Similar age-effect analyses can be performed on the mean and dispersion of the flyby distance amplitude distributions (Fig 2C, Supp. Fig S3 E,F). The means of P400 but not P1-flyby distances reduced with age for left, right and central faces, suggesting that on an average, trials in older infants passed closer to P400-template than those in young infants. ($r = -0.37$, $p<0.02$, $r=-0.52$, $p<0.006$, $r = -0.26$, $p <0.06$ for left, right and central faces respectively). While the mean distances reduced with age, the trial variability (S.D.) of distance to P400 (but not to P1) template increased with age -- for all conditions (left faces: $r = 0.42$, $p<0.003$; right faces: $r = 0.34$, $p<0.02$ and central faces: $r = 0.53$, $p<0.007$)). This suggests that even though trials on an average passed closer to P400 template, they remained more flexible in how far or close they could fly from their respective baseline close to this template. For P400-flybys, these trends continued well into the adulthood, i.e., trials passed on average much closer to the template but trial variability remained higher for adults than for all infants (Fig 2 C, right box insets and Fig S3 E, F box-plots and table 1). These results suggest a common mechanism for the maturation of flyby-distances around P400, not affected by differential maturation of hemispheres.

To summarize, single-trial event-related dynamics significantly changes with age: it becomes in general more fluid (faster and relatively more variable in timing or distance of approach), is specifically affected by the event it approaches (P1 or P400) and in case of infants, by the hemisphere probed by the lateralized stimulus, thus probably by its maturational stage.

bioRxiv preprint doi: https://doi.org/10.1101/2021.03.07.434162; this version posted March 8, 2021. The copyright holder for this preprint (which was not certified by peer review) is the author/funder. All rights reserved. No reuse allowed without permission.

4) Between-trial variability quenching (VQ) after stimulus presentation

Irrespective of their approach to the templates, trials can remain far or close to each other at any point. Hence, as the second approach at characterizing ERV, we investigated between-trial variability (i.e., how tight or loose is the flight formation of the bird flock, see *Methods*). We observed a significant post-stimulus decrease in the between trial variability for all task-conditions and for both infants and adults (Blue plots in Fig 3A-B, sup Fig S4). For infants, between-trial variability significantly remained 1-2 standard deviations lower than the average baseline variability ~200-700 ms post-stimulus ($p < 0.001$ for left, right faces and $p<0.003$ for the central faces), while in adults, significant VQ occurred ~150-500 ms ($p<0.005$), similar to the duration previously reported for variability quenching in aduts(Schurger *et al.*, 2015).

Between-trials variability quenching is not automatically induced by ERP component flybys: The latency of the largest post-stimulus quenching (lowest variability) significantly differed across age-groups and task conditions. Strikingly, for lateralized faces, the latency of the significant VQ coincided with the latency of the closest P1-flyby in the youngest infants (First trimester: 5-12 week-olds, N=14) whereas in the older infants (Second Trimester: 16-24 weeks, N=13), the moments of VQ co-occurred with the P400-flyby (Fig 3 A). In other words, in younger infants, the trials "flight formation" remained on an average more compact when flying by the P1-template (significant VQ times: 204-352 ms, window of closest P1-flyby: 175-400 ms). By contrast, in older infants, trials remained the closest to each other when passing near the P400-template (significant VQ: 432 – 616 ms, closest P400-flyby: 432-620 ms).

Importantly, the absence of between-trial VQ did not imply absence of a flyby. Indeed, in first-trimester infants, trials still had a marked P400-flyby even when there was no between-trial VQ at the corresponding latency. Analogously, there was still a P1-flyby for second-

bioRxiv preprint doi: https://doi.org/10.1101/2021.03.07.434162; this version posted March 8, 2021. The copyright holder for this preprint (which was not certified by peer review) is the author/funder. All rights reserved. No reuse allowed without permission.

trimester infants despite the lack of a P1 VQ. These effects were consistent for both left and right face presentation (Fig S4A-B). Thus, flying by an ERP component appears to be a necessary but not a sufficient condition for between-trial VQ. In adults too, a single window of VQ coincided with the P400-flyby, similar to the second-trimester infants' pattern (Fig 3C, Fig S4 C, and D). However, the VQ was much larger in adults than in infants, trials remaining significantly close to each other during the entire duration of the P400-flyby (significant VQ: 140 – 460 ms, P400-Flyby: 120-528 ms). Moreover, variability around P1-flyby was significantly higher in adults than in young and old infants. By contrast, the variability around P400-flyby was significantly higher in young infants than in both older infants and adults (box plots in Fig 3D, stats: table 2).

Between-trials variability quenching depends on both stimulus configuration and age: The temporal shift of the between-trials VQ, from P1 to P400 gives the first proof of a change in the ongoing dynamics occurring over the first semester of life. However, such a shift may also be due to the structural changes in the peripheral visual pathway and V1 which are known to reach a milestone at this precise age (Braddick and Atkinson, 2011; Adibpour, Dubois and Dehaene-Lambertz, 2018). To investigate the possible origin of such a shift, we repeated the same analysis in the subset of infants who were also presented with central faces (Fig 3B). We found that the VQ at P1 but not P400-flyby significantly differed within the same infants for the two different face stimuli configurations (Wilcoxon signed rank (z)=58, $p<0.025$ for P1, $z=123, p>0.92$ for P400). Interestingly, when presenting central face stimuli, the VQ co-occurred with the P400-flyby even for 5-12 weeks infants, similarly to the response to lateral faces observed in 16-24 weeks infants. Fig 3C summarizes the time-ranges of between-trials variability quenching and P1/P400-flybys across all age groups and experimental conditions ($p<0.05$, all analyses were corrected for multiple comparison and temporal independence using one-sided cluster-based permutation t-test).

bioRxiv preprint doi: https://doi.org/10.1101/2021.03.07.434162; this version posted March 8, 2021. The copyright holder for this preprint (which was not certified by peer review) is the author/funder. All rights reserved. No reuse allowed without permission.

Nevertheless, age quantitatively affected the strength of inter-trial variability quenching events. As expected from the observed inter-group differences, we found a linear increase of the strength of between-trials variability quenching with age at the P400-flyby latency mainly for lateral faces but not for central faces (Fig 3D bottom panel, $r = -0.43$, $p < 0.003$ for left faces; $r = -0.30$, $p < 0.03$ for right faces; $r = -0.13$, $p < 0.3$ for central faces), further confirming the qualitative differences observed in quenching dynamics for different stimuli configurations. Table 2 compares infants with adults.

In summary, these results collectively prove the existence of a rich temporal structure in the dynamics of between-trials variability, qualitatively and quantitatively maturating over the first semester post-term birth. Such dynamics follows a different maturation trajectory than ERPs and in the same infants its temporal structure can be modulated depending on the task at hand. Moreover we observe that such quenching was spatially global phenomena (suppl. Text, Fig S5).

5) Age-related increase and structure of within-trial variability

Our third and last strategy was the analysis of within-trial variability (i.e., how and when individual birds within the flock modify their speed of flight). For this, we quantified how the topography of activations evolved from one time-point to the next – i.e. the distance traveled in the space of possible activity topographies –over a unit time, hence reinterpreted as a measure of the within-trial speed in the topographic activity space (see *Methods*). Thus, topographies of activations which are stable over time and fluctuate very little from one moment to the next yield instantaneous within-trial variability close to zero. Conversely, abrupt changes of topographies occurring at specific instants –as e.g. eventual switching between microstates(Michel and Koenig, 2018) – would map to sudden increases of the instantaneous within-trial speed.

bioRxiv preprint doi: https://doi.org/10.1101/2021.03.07.434162; this version posted March 8, 2021. The copyright holder for this preprint (which was not certified by peer review) is the author/funder. All rights reserved. No reuse allowed without permission.

Absolute within-trial variability increases with age: We observed a significant positive age-effect on the average absolute within-trial speed across all epochs irrespective of the task condition (Fig 4 A for lateral faces: r= 0.38, p<0.01; Fig S6 A for central faces: r=0.56, p<0.009). The relationship between age and within-trial speed extended further to adults as well; i.e. within-trial speed of adults was significantly higher compared to infants (box plot in Fig 4A, H= 24.33, p<10^-5, Kruskal-Wallis test, Absolute within-trial speed (correlation distance a.u.*10^-3) for 5-12 wo: 7.65 ± 1.63 and for 16-24 wo: 11.17 ± 3.49 and for adults: 15.82 ± 2.87) and for an individual adult, strikingly similar across task conditions (p>0.1 for all individual condition-wise differences, Wilcoxon-ranksum test). These results suggest that large-scale fluctuations of brain-states become globally more variable with age irrespective of task (i.e., birds within the flock move more swiftly). Interestingly, we also observed that distributions of instantaneous within-trial speed were heavy-tailed for both infants and adults (Supplementary Text, Fig S6 A, and S6D).

The structure of speed profiles around ERP flybys is modulated by age: Instead of looking at within-trial speed during entire duration of trials, it is interesting to understand how it is specifically modulated during the approach to known evoked ERP components (e.g., what are the speeds of individual birds flying close to the poles). We performed flyby-triggered averages of within trial speeds by pulling together all individual events of closest flyby to templates(sometimes multiple events per trial) and averaging within-trial speed in 800-ms window around these events (peri-fly-by speed profiles, Fig 4B, see *Methods*). Fig 4 C, D shows average within-trial speed in the vicinity of respectively P1 and P400-flybys for lateral faces (Fig S6 B for central faces). In these profiles, peaks and troughs of within-trial speed are clearly visible, distributed symmetrically around the flyby time, and tend to get more marked with age. Irrespective of their absolute within-trial speed, on an average, trials transiently slowed down around both P1 and P400-flybys, but for all conditions and age-

bioRxiv preprint doi: https://doi.org/10.1101/2021.03.07.434162; this version posted March 8, 2021. The copyright holder for this preprint (which was not certified by peer review) is the author/funder. All rights reserved. No reuse allowed without permission.

groups with a larger slowing down around P400-flyby than for P1 (condition wise signed rank test: H=30, p<0.001, H=55,p<10^-5 and H =1.0,p<0.0005 for infant central, lateral and adults lateral faces respectively). Given that the overall within-trial speeds increased with maturation, it was remarkable that, in the vicinity of P400-flybys, trial speed decreased ~2 S.D. below the average speed for both young and old infants (e.g., individual birds fly overall faster, but noticeably slowing down around the specific poles). Adults looking at lateralized faces showed a similar qualitative speed profile, but within-trial slowing down around P1-flybys was no longer significant, while the slowing down around P400-flyby was even more pronounced than in second trimester infants (Fig 4C,D dashed green lines).

These characteristic speed profiles are reminiscent of the accelerations and decelerations that a physical ball would experience when rolling on a surface with different potential energy landscape (accelerating while descending into the valley and decelerating while ascending out of the valley due to gravity, Fig. 4 E & F). It is thus tempting to interpret these speed profiles as reflecting the influence of a "force field" getting more intense with increasing age, a set of control influences on system's trajectory manifested while approaching critical points.

To quantify age-effect, we extracted for each infant the peak and trough of the relative within-trial speed in the ~100 ms windows centered and aligned to flybys. Despite transient slowing down at P1, it was the amount of peri-flyby speed increase after P1 flyby (the peaks in the speed profile) that positively correlated with age for lateral but not central faces (r= 0.41, p<0.005, Fig 4G, Fig S6 D, E for left and right faces respectively). In contrast, for P400 flybys, for both central and lateral faces, it is the depth of the speed trough that augmented with age, associated to a more marked slowed down (r = -0.43, p<0.003, Fig 4H; see Fig S6 C,D for the left and right faces separated). Table 3 summarizes the significant time-clusters of group-level fly-by triggered speed differences.

bioRxiv preprint doi: https://doi.org/10.1101/2021.03.07.434162; this version posted March 8, 2021. The copyright holder for this preprint (which was not certified by peer review) is the author/funder. All rights reserved. No reuse allowed without permission.

To conclude, we observed a characteristic slowing down and speeding up of single-trials at the time of their closest flybys to the known ERP templates that differed with age and task conditions. While overall within-trial state fluctuations increased with age, we saw age-dependent decrease of within-trial variability around P400 flyby where between-trial variability found its minima. We show that these modulations of between and within-trial variability were independent of the overall signal-to-noise ratio as measured by L2-norm (Fig S7, supplementary text).

DISCUSSION

In this study, we demonstrate the existence of a rich temporal organization of response variability in adults and infants, apart from the already known temporal structure of the response means (i.e. Event Related Potentials (ERPs)). We thus propose the concept of Event-Related Variability (ERV), generalizing the ERPs, to refer to the temporally structured dynamics of response fluctuations. To characterize ERV, we focused on the complementary aspects of: single-trial (dis-)similarity to known ERP components (ERP flyby analyses, Fig. 2); reproducibility of response trajectories across different trials (between-trials variability analyses, Fig. 3); and, changing rate of reconfiguration of the induced activity topographies along individual trials (within-trial speed analyses, Fig. 4). Our results confirm that for both infants and adults, the trial variability remains very large (absolute correlation distances of order ~0.95, hence Pearson coefficient ~ 0.05) and yet this variability is significantly modulated by the face presentation. In all conditions, an epoch of enhanced trajectory reproducibility (decreased variability) is detected after stimulus presentation, confirming many previous reports in adults(Churchland *et al.*, 2010; Schurger *et al.*, 2015). Beyond these previous studies, we observe that the latency of between-trial variability quenching evolves through age and that, at a given age, is strongly modified by the task at hand.

bioRxiv preprint doi: https://doi.org/10.1101/2021.03.07.434162; this version posted March 8, 2021. The copyright holder for this preprint (which was not certified by peer review) is the author/funder. All rights reserved. No reuse allowed without permission.

Furthermore, we observe that enhancements of trial reproducibility always occur in time ranges in which trials tend to fly at a closer-than-average distance from an ERP template. The opposite however is not true, establishing ERP flybys and between-trials variability quenching as partly independent phenomena. The fact that some flybys co-occur with a between-trials variability quenching and some others not suggest that there are different ways to approach an ERP component. When there is no simultaneous between-trials variability quenching, trials get close to a specific activity configuration (reminiscent of the target ERP component template) but do it every time in a rather unconstrained fashion (e.g. one bird may fly by the same pole coming from a nearby roof and some other from a tree far away). On the contrary, when there is a simultaneous quenching, a specific path of approach is followed more faithfully (e.g. birds that would approach the pole always flying southward along the power line).

Does variability quenching denote top-down processes?

Various elements suggest that quenching events are not a mere automatic consequence of stimulus presentation, but may be the signature of a more efficient control exerted on the system's trajectory, possibly implementing a form of top-down regulation: First, quenching can occur even late, after the stimulus onset e.g. in older infants, for whom quenching occurs during the P400 time-window. Second, age does not simply extend the time-window of quenching but shifts its target from P1 to P400 and third, even at a given age, the quenching dynamics can be qualitatively modified by even small changes in the stimulation. First-trimester infants show P1-component flybys when presented with both central and lateral faces; however variability quenching at this flyby occurs only for the latter. These observations suggest that the presence or absence of quenching might reflect the difficulty of the task. Indeed, lateral faces are more difficult to perceive for infants, because of the competition of the lateral face with the central attractor in our experimental paradigm, but

bioRxiv preprint doi: https://doi.org/10.1101/2021.03.07.434162; this version posted March 8, 2021. The copyright holder for this preprint (which was not certified by peer review) is the author/funder. All rights reserved. No reuse allowed without permission.

also due to slower maturation of parafovea compared to fovea(ALLEN, TYLER and NORCIA, 1996). Thus, a quenching event where the system's dynamics is channeled along a specific track might reflect a requirement for a more intensive information processing than what is possible when just realizing a "hit and run" visit to a P1-component. Such an improved control on trajectories could be achieved via top-down regulatory mechanisms, whose existence in infants has been confirmed experimentally(Emberson, Richards and Aslin, 2015; Kouider *et al.*, 2015; Kabdebon and Dehaene-Lambertz, 2019).

The shift of focus for variability quenching, from P1 to P400 at ~12 weeks (for lateral faces) corresponds to an age when vision improves considerably. The end of the first trimester represents a first landmark in visual development when several peripheral structures reach maturity (e.g. lens, fovea) and myelination of the optical fibers and maturation of V1 reach a plateau after a period of rapid change. The latency for visual P1 for central faces converges to adult values already at 12 weeks(Dubois *et al.*, 2008), while peripheral vision matures more slowly(ALLEN, TYLER and NORCIA, 1996). Feed-back connectivity is also progressively restructured, passing from disperse growth to selective pruning (Kennedy *et al.*, 2007) which may allow for more effective attention control or predictive influences. Thus, to disentangle between bottom-up and top-down contributions to this phenomena, future studies will have to analyze ERV dynamics and its remodeling in tasks in which difficulty and information processing load can be parametrically adjusted.

Our developmental dataset allowed determining that already at the end of the first trimester of life; the flyby dynamics and between-trials variability in infants have reached a temporal organization qualitatively analogous to that of the adult subjects. Such an early emergence of an adult-like ERV, suggests that ERV structure is a feature of cognitive architectures conferring fundamental advantages. Acquiring the capacity to actively modulate the level of the internal state fluctuations might be instrumental in efficient perception and

bioRxiv preprint doi: https://doi.org/10.1101/2021.03.07.434162; this version posted March 8, 2021. The copyright holder for this preprint (which was not certified by peer review) is the author/funder. All rights reserved. No reuse allowed without permission.

behavior. The role of higher-level representations have been recently emphasized challenging the classical purely bottom-up view of learning(Tenenbaum *et al.*, 2011). In this perspective, functional architectures should involve specific computations at different levels of a processing hierarchy but also allow the upper-level to constrain lower-level learning. Note that overall fluctuations are not suppressed by development, but actually boosted (cf. Fig. 4A), as we found in agreement with other reports(McIntosh, Kovacevic and Itier, 2008) . Such enhanced variability could stem from the learning of richer models of a complex environment, encoded in the statistical structure of intrinsic activity fluctuations, or from a better sampling of these internal models(Ma *et al.*, 2006; Berkes *et al.*, 2011). At the same time, if the specific computations are more difficult or longer to perform, they may require the transient stabilization of specific dynamical modes –which are not necessarily point attractors(La Camera, Fontanini and Mazzucato, 2019)– enabling suitable modes of information routing or processing(Palmigiano *et al.*, 2017; Clawson *et al.*, 2019). To efficiently perform task-related processing, the system should thus be able to switch between large variability epochs –facilitating inference and exploration– and consistently reproducible metastable states, as possibly indicated by variability quenching events at more computation-intensive task stages.

Within-Trial Variability Modulation

Response variability modulation events also take place within individual trials in both infants and adults confirming and extending previous results on adults(Schurger *et al.*, 2015). If a between-trial variability quenching event denotes that system's trajectories follow a specific "flux tube" to reach and leave an ERP component ,the phenomenon of within-trial slowing-down suggests that the flow of *each of the individual trajectories* within this tube characteristically decelerates when the system approaches certain landmarks (ERP component flyby). This is important, because perception and cognition happen in real time

bioRxiv preprint doi: https://doi.org/10.1101/2021.03.07.434162; this version posted March 8, 2021. The copyright holder for this preprint (which was not certified by peer review) is the author/funder. All rights reserved. No reuse allowed without permission.

(one cannot rely on averaging multiple stimulus presentations before perceiving a face). Therefore, modulations of response variability can be instrumental only if they occur within individual trials. Eventually, the slight slowing-down of individual trials near the time of P1 and, in a particularly marked way P400 flybys, correspond to the system trajectories lingering around the corresponding ERP template for a short time. During this time, the trajectories are thus bounded and this transient reduction in the fluctuations could be detected, e.g., by an integrator neuron –serving as a tempotron readout(Gütig and Sompolinsky, 2006)– to signal that a given stage in cognitive processing has been reached and thus initiate the next processing step in a sequence(Zylberberg *et al.*, 2011).

However, even when between-trial variability is at its minima, within-trial fluctuations are not completely suppressed. In other words, flyby and quenching events do not correspond to moments of freezing but trajectories rather keep their rich dynamics. This is reminiscent of reservoir computing paradigms(Maass, Natschläger and Markram, 2002) in which the chaotic spontaneous fluctuations are only transiently reduced by the applied inputs and are actually needed to boost learning capabilities. The evolution of the system seems thus always far from being at a stable attractor. Three possible mechanisms have been suggested previously for variability reduction: post-stimulus transient strengthening of one of the many possible attractors(Litwin-Kumar and Doiron, 2012), chaos suppression(Rajan, Abbott and Sompolinsky, 2010) or "supra-linear stabilization"(Hennequin *et al.*, 2018) of mostly unstable system, where amplitude fluctuations due to recurrent excitation are damped at certain post-stimulus moments due to increased inhibitory feedback. The last two theoretical arguments seem to be better compliant with our current observations. Additional computational investigation will be needed to disambiguate which of the possible scenarios is leading to the observed quenching. Indeed, different models may predict different statistical distributions of secondary features –such as e.g. the jitter in latencies to flybys– to compare

bioRxiv preprint doi: https://doi.org/10.1101/2021.03.07.434162; this version posted March 8, 2021. The copyright holder for this preprint (which was not certified by peer review) is the author/funder. All rights reserved. No reuse allowed without permission.

with the empirically measured ones. Furthermore, parameters such as the local excitation/inhibition balance within cortical populations evolve with age(Hensch and Fagiolini, 2005) and the maturation of these parameters may predict different ERV developmental trajectories depending on the actual dynamic mechanism.

Besides reductions, we also observe transient increases of within-trial variability. The system approaching a flyby event initially accelerates and then sharply decelerates before accelerating to reach the mean speed again. If these variations of speed had to be explained as due to motion in a force field, the free energy minimum of this landscape would be located at the first maximum of speed, preceding the ERP component flyby ~50-100 ms; depending on the component and condition. On the contrary the ERP template is more closely reproduced at the within-trial speed minima. In our energy landscape metaphor, decelerations would signify leaving an attractor valley, while the system crosses the high energy barrier and accelerates to enter another valley. In this view, the manifestation of an ERP component would signal the moment of crossing from one critical point to the next. Such conjecture may be potentially validated by estimating the morphology of an effective free energy landscape surrounding the ERP templates(Ezaki *et al.*, 2017). Another possibility is that system's evolution is "itinerant", i.e. Approaching a critical point along a stable low-dimensional manifold (e.g. a flow line), slowing down as the critical point is approached, but then repelled again away along a different unstable manifold, accelerating toward a different critical point(Tsuda, 2009). These observations are compliant with the framework of statistical physics of complex systems(Skarda and Freeman, 1987; Pillai and Jirsa, 2017). In which, changes of ERV dynamics through development and learning would be accounted for by the growth of more marked barriers and sinks in an effective energy landscape or bifurcations causing the birth, fusion or death of different attractors or saddle points in the system's high dimensional phase space.

bioRxiv preprint doi: https://doi.org/10.1101/2021.03.07.434162; this version posted March 8, 2021. The copyright holder for this preprint (which was not certified by peer review) is the author/funder. All rights reserved. No reuse allowed without permission.

Our approach has methodological limitations that could be overcome by future developments. For instance, the extraction of ERP templates in our case depended on a manual inspection, but more sophisticated algorithms for the temporal clustering of single-trial ERP topographies(Vahid *et al.*, 2020) could be used and combined with our variability analyses schemes. The occurrence of large within-trial variations also need to be put in correspondence with microstate transitions or other approaches to describe ongoing dynamics of intrinsic functional connectivity(Lombardo *et al.*, 2020) which also reveal power-law distributed statistics of fluctuations. Finally, linking activity to network state dynamics may allow assessing whether exchange of information is dominated by bottom-up or top-down flows at different ages or ERP stages(Bastos *et al.*, 2015).

In conclusion, ERPs have been an attractive description of the post-stimulus brain activity, described as successive steps defined by their reproducible latency and brain sources, and thus made possible to obtain neural algorithms underlying cognition. However, this description was somewhat misleading, ignoring the ongoing activity. The framework proposed here encompasses both aspects. We recovered that ERP components are “special dynamical points” for the on-going activity, confirming that ERPs are indeed capturing neural consequences of a stimulus presentation. At the same time, we also showed that they are far from capturing the entire activity patterns following a stimulus. We proposed the term ERV, as a better concept to describe the neural consequences of a stimulus. This proposal is not purely semantic, since it allows describing in integrated manner ERP maturation on one hand and the enhancement and structured variability of the background EEG on the other, speculating that the gradual change of ongoing activity might reflect the increasing knowledge of the environment over development.

bioRxiv preprint doi: https://doi.org/10.1101/2021.03.07.434162; this version posted March 8, 2021. The copyright holder for this preprint (which was not certified by peer review) is the author/funder. All rights reserved. No reuse allowed without permission.

ACKNOWLEDGMENTS

This research was supported by grants from the Fondation NrJ, from the European Research Council (ERC) under the European Union's Horizon 2020 research and innovation program (grant agreement No. 695710), and from the Fondation de France (call Neurodevelopment and Autism 2012). This work, carried out in part within the Institut Convergence ILCB (ANR-16-CONV-0002), has benefited from support from the French government, managed by the French National Agency for Research (ANR) and the Excellence Initiative of Aix-Marseille University (A*MIDEX).

AUTHOR CONTRIBUTIONS

SN performed all computational analyses, PA, JD and GDL designed the initial ERP study, collected EEG recordings and preprocessed the signals, SN, GDL and DB designed the actual study, and wrote the initial manuscript, and all authors reviewed the manuscript.

DECLARATION OF INTERESTS

The authors declare no competing interests.

bioRxiv preprint doi: https://doi.org/10.1101/2021.03.07.434162; this version posted March 8, 2021. The copyright holder for this preprint (which was not certified by peer review) is the author/funder. All rights reserved. No reuse allowed without permission.

MAIN FIGURE TITLES AND LEGENDS

Fig 1 Task Paradigm and Variability in Event Related Potentials. A) Infants (and adults) were presented with unfamiliar faces consecutively in the left and right hemi-field. A subset of infants was also presented with faces in center. **B)** Grand Average voltage topographies for the three conditions for infants. Early (P1) and late (P400) ERP components (marked with orange and green horizontal bars respectively) are visible for each condition. **C)** Example voltage time-courses averaged across right occipital electrodes for one representative infant (age =12.1 weeks) for faces presented in the left hemi-field. Amplitude and latency of single-trial responses (blue lines) are highly variable in comparison with average ERP response (red lines). Single-trial voltage topographies in the P1 and P400 response range are notably different from the grand average ERP topography. **D)** Trajectory of continuous time-segment (~ 12 s) reduced to 3-dimensional PC space from 128-channel EEG sensor space for one example infant. Each point corresponds to a single instantaneous topographic pattern of the raw data. Time-points falling in 450-500 ms post-stimulus time range are marked in red. **E)** Schematic summary of the methods used to gauge single-trial variability: Fly-by to ERP template, Between-trial variability and Within-trial speed.

bioRxiv preprint doi: https://doi.org/10.1101/2021.03.07.434162; this version posted March 8, 2021. The copyright holder for this preprint (which was not certified by peer review) is the author/funder. All rights reserved. No reuse allowed without permission.

Fig 2 Maturation of single-trial Fly-by statistics for faces presented on the right hemi-field. A) Average flyby distances to P1 (left) and P400 (right) ERP templates (as shown on top) for each infant. Each row represents a single infant, sorted in ascending order according to their age (from youngest = 5.6 weeks to oldest=23.1 weeks). Red vertical lines emphasize the reduction in average flyby distance from ~150-350 ms for P1 and ~400-600ms for P400 templates. The slopes of red lines suggest that latency of closest distance reduces with age. **B**) Median flyby latency significantly decreased with age for both P1 (top left) and P400-flyby (top right panel). At the same time, S.D. of single-trial flyby latencies significantly increased with age for P1 (bottom left panel) and showed a negative trend with age for P400 template (bottom right panel). Inset box-plots represent the same statistics for adults. **C**) Average flyby distances to P1 template showed non-significant increase with age (top left panel), while the same for P400 template decreased with age (top right panel). At the same time, S.D. in single-trial flyby distance distribution for both P1 (bottom left panel) and P400 templates (bottom right panel) increased with age. Box-plots show the distributions for adults. Adults followed the same trend on P400 template flyby distance statistics. Shaded areas indicate 95% confidence interval for the slope of the least square fitting line, all r-values corrected for multiple comparisons with 1-tailed permutation t-test).

bioRxiv preprint doi: https://doi.org/10.1101/2021.03.07.434162; this version posted March 8, 2021. The copyright holder for this preprint (which was not certified by peer review) is the author/funder. All rights reserved. No reuse allowed without permission.

Fig 3 Maturation of Between-trial variability and its relation to Fly-by distances.

A) Group average between-trial correlation distance (blue curves, Z-scored) for 5-12 weeks (N= 14, top panel) and 16-24 weeks (N= 13, bottom panel) old infants plotted together with grand-average flyby distances (Z-scored) to P1 (red line) and P400 templates (orange line), for the lateral faces. Significant reduction in between-trial variability coincides with the closest-flyby to P1-template for young infants (top panel), and with the P400-template for old infants (bottom panel). **B)** For central faces, significant between-trial variability (blue line) reduction coincides with P400-flyby (orange line) for both groups. Shaded areas indicate standard error to the mean. **C**) Significant clusters of variability and flyby distance reductions for all conditions and groups (Horizontal bars indicate timepoints of significant reductions from mean; $p<0.05$, all corrected for temporal non-independence using cluster-based permutation t-test). Boxes highlight the correspondence between clusters of between-trial variability and P1/P400 flyby distance reductions in the different conditions. 16-24 weeks infants qualitatively look similar to adults. 5-12 weeks infants when presented with central faces also quench variability at P400. **D)** Between-trial variability during P1-flyby increases with age (top) while the same during P400-flyby decreases with age for lateral but not central faces. (All r-values corrected for multiple comparison with one-tailed permutation test). Shaded area indicates 95 % confidence interval for the slope estimation of the least square fitting. Box-plots show between-trial variability distributions for adults.

bioRxiv preprint doi: https://doi.org/10.1101/2021.03.07.434162; this version posted March 8, 2021. The copyright holder for this preprint (which was not certified by peer review) is the author/funder. All rights reserved. No reuse allowed without permission.

Fig 4 Maturation of Within-trial Speed for lateral faces.

A) Instantaneous within-trial speed or moment-to-moment fluctuations (averaged across all trials and timepoints per subject for lateral faces) significantly increased with age. Each dot represents one infant; box-plot represents average speed distribution for adults. Shaded regions indicate 95 % c.i. for slope estimates. **B)** Trial speed around flyby to P1 and P400-like templates for each subject was extracted by considering within-trial speed (i.e. correlation distance between topographies from one time-point and next) in 800 ms time-window around the closest 5 % flyby distances to the respective template. **C**) Group averaged trial speed profiles around P1 and **D**) P400 flybys for different age-groups. Instantaneous speed transiently reduced while approaching P1 and P400 like states. Significant speed difference existed between 5-12 weeks and 16-24 weeks old infants as indicated by black horizontal bars, cluster based permutation t-test, $p<0.05$) (**E & F)** Energy landscapes that might underlie the speed profiles for P1 and P400 templates respectively (metaphorically resembling to a ball crossing a hill). Peaks and troughs around the flyby templates become more marked for 16-24 weeks old infants (dotted lines) as compared to 5-12 weeks old infants (solid lines). (**G**) Peak trial speed in 100 ms time-window around P1-flyby and (**H**) Lowest trial speed in 100 ms time-window around P400-flyby for lateral faces. Box-plots represent the same speed distribution for adults. Instantaneous trial speed around P1-flyby significantly increased with age while the same around P400-flyby significantly reduced with age with older infants already showing profile similar to adults.

bioRxiv preprint doi: https://doi.org/10.1101/2021.03.07.434162; this version posted March 8, 2021. The copyright holder for this preprint (which was not certified by peer review) is the author/funder. All rights reserved. No reuse allowed without permission.

MAIN TABLES AND LEGENDS

Table 1	**Comparison of P1 and P400 Flyby Mean Amplitude Across Age-Groups**	
	Left Faces	**Right Faces**
P1	H = 11.48, p=0.003	H = 9.76, p=0.007
	5-12wo vs 16-24 wo: n.s.	5-12 wo vs 16-24 wo: n.s.
	16-24 wo vs adults: p= 0.015	16-24 wo vs adults: 0.072 n.s.
	5-12 wo vs adults: p= 0.009	5-12 wo vs adults: p=0.014
P400	H = 13.29 p = 0.0013	H=13.47,p=0.001
	5-12wo vs 16-24 wo: p = 0.18 n.s.	5-12 wo vs 16-24 wo: p= 0.4 n.s.
	16-24 wo vs adults: p = 0.25 n.s.	16-24 wo vs adults: p =0.028
	5-12 wo vs adults: p = 0.001	5-12 wo vs adults: p= 0.003

Table 1 Average closest flyby distances across age-groups (5-12 week old: first trimester infants, 16-24 weeks old trimester infants and adults) were compared using separate Kruskal-Wallis tests for different ERP templates (P1, P400 responses) and for faces presented in the left and right hemi-field. The main effects are reported before post-hoc Mann-Whitney U-test for pair-wise comparisons. P values are corrected for multiple comparisons using Bonferroni correction.

bioRxiv preprint doi: https://doi.org/10.1101/2021.03.07.434162; this version posted March 8, 2021. The copyright holder for this preprint (which was not certified by peer review) is the author/funder. All rights reserved. No reuse allowed without permission.

Table 2	**Age Difference in Between-trial Variability around Flybys (z-scores)**	
	Left Faces	**Right Faces**
P1	H = 11.72,p<0.003 5-12 wo vs 16-24 wo: p=0.25 n.s. 16-24 wo vs adults: p = 0.229 n.s. 5-12 wo vs adults: p =0.003	H = 12.95, p=0.001 5-12 wo vs 16-24 wo: p=0.5 n.s. 16-24 wo vs adults: p = 0.05 5-12 wo vs adults: p =0.002
P400	H = 16.68 p=0.0002 5-12wo vs 16-24 wo: p =0.001 16-24 wo vs adults: p>0.8 n.s. 5-12 wo vs adults: p = 0.001	H=14.10 ,p= 0.0009 5-12 wo vs 16-24 wo: p= 0.08 n.s. 16-24 wo vs adults: p = 0.1 n.s. 5-12 wo vs adults: p=0.002

Table 2 Between-trial variability (z-scores) were compared the three age-groups (5-12 week old: first trimester infants, 16-24 weeks old trimester infants and adults) in their respective moments of P1 and P400 closest flybys using separate Kruskal-Wallis tests for different ERP templates (P1, P400) and for faces presented in the left and right hemi-field. The main effects are reported before post-hoc Mann-Whitney U-test for pair-wise comparisons. P-values are corrected for multiple comparisons using Bonferroni correction.

bioRxiv preprint doi: https://doi.org/10.1101/2021.03.07.434162; this version posted March 8, 2021. The copyright holder for this preprint (which was not certified by peer review) is the author/funder. All rights reserved. No reuse allowed without permission.

Table 3: Age-differences in Within-Trial Variability Around Flybys		
	Left Faces	**Right Faces**
P1	S.C.: None	S.C.: [8 80] ms, H=6.07, p=0.048 5-12 wo vs 16-24 wo: p = 0.08 16-24 wo vs adults: p = n.s. 5-12 wo vs adults: p =0.17
P400	S.C.: [-384 -308] ms: H = 14.87, p= 0.0006 5-12wo vs 16-24 wo: p = n.s 16-24 wo vs adults: p= 0.0008 5-12 wo vs adults: p= 0.008	S.C.[-400 -268]ms, H=14.42, p=0.0007, 5-12wo vs 16-24 wo: p = n.s 16-24 wo vs adults: p= 0.0005 5-12 wo vs adults: p= 0.015
	S.C = Significant Clusters (p<0.05, cluster based permutation tests)	S.C.[-72 -12]ms, H= 16.266, p=0.0003 5-12wo vs 16-24 wo: p = n.s. 16-24 wo vs adults: p= 0.03 5-12 wo vs adults: p= 0.0003

Table 3 Fly-by triggered within-trial speed profile time-series (z-scores) across the three age-groups were compared using cluster-based permutation F-tests separately for each ERP template and for each hemi-field to find the significant time clusters ($p<0.05$). During post-hoc analyses, average within-trial speed in these significant time-windows was compared using Kruskal-Wallis test. Pair-wise comparisons were tested using Mann-Whitney U-test. P-values are corrected for Bonferroni correction.

MATERIALS AND METHODS

Subjects

Reported results included data from two cohorts. The first group of healthy full-term infants (N = 39, Mean age: 14.15 ± 4.79 weeks, age range: 5.6 to 23.6 weeks, 11 girls) was studied elsewhere to investigate the functional maturation of visual Event Related Potentials (ERP) to lateralized faces(Adibpour, Dubois and Dehaene-Lambertz, 2018). A subset of these infants (N = 22, Mean age: 14 ± 4.96 weeks, age range: 5.6-22 weeks, 7 girls) was also tested

bioRxiv preprint doi: https://doi.org/10.1101/2021.03.07.434162; this version posted March 8, 2021. The copyright holder for this preprint (which was not certified by peer review) is the author/funder. All rights reserved. No reuse allowed without permission.

to study ERP responses to central faces. To compare the results obtained for infants with adults, we additionally included the second group of young adults (N= 13, Mean age: 23.39 ± 2.32 years, age range: 21 to 27.1 years, 6 females) who were presented with the lateralized faces following the same paradigm as infants. The study was approved by the ethical committee for biomedical research. All adult subjects and parents of infants gave written informed consents before participating in the study.

Task Paradigm and Protocol

Lateralized Faces. Each trial started by a rotating colored bull's-eye that remained at the centre of the screen during the whole experiment to attract infants' attention to the center of the screen. Streams of face images (male or female face out of 6 neutral, unfamiliar front faces) appeared consecutively on the left and right side of the bull's eye for 250 ms followed by a variable delay between images (550 to 950 ms post-offset of the image with a 50-ms step). The asynchronous presentation ensured minimal anticipatory gaze to the left or right side. To investigate the inter-hemispheric transfer of information in infants, each stream included three types of images: a side-assigned face image (standard), a novel face (new-deviant), or the face commonly assigned to the other side (known-deviant), with the expectations that an efficient inter-hemispheric transfer ensures ERP response to known-deviant faces to be similar to standard faces. Each block included ~80 % standard, ~10 % new-deviant and ~10 % known-deviant faces. For the current analyses however we considered all faces presented on either left or right side; irrespective of this distinction.

Central Faces. One female and one male face, not used during the lateralized paradigm, were presented at the centre of the screen for 250 ms, spaced by a random interval of 550-950 ms during which the colored bull's eye was presented.

bioRxiv preprint doi: https://doi.org/10.1101/2021.03.07.434162; this version posted March 8, 2021. The copyright holder for this preprint (which was not certified by peer review) is the author/funder. All rights reserved. No reuse allowed without permission.

EEG Protocol and Pre-Processing. EEG recordings were acquired with EGI net comprising 128 electrodes for infants and GSN net comprising 256 electrodes for adults and digitized in real-time at a sampling rate of 250ms. EEG data was further pre-processed in EEGLAB software. Recordings were band-pass filtered between 0.5 and 20 Hz, the signal was segmented into epochs of 1.7 s (−0.2 to 1.5s relative to the onset of face presentation). Channels and trials contaminated by motion or eye-blink artifacts were rejected. For infants, additional trials were rejected when the eye-gaze moved away from the screen; by manual inspection of video-recordings. Epochs were re-referenced by reference averaging but no baseline correction was applied to allow unbiased analyses of post-stimulus variability as compared to pre-stimulus variability. Finally, EEG topographies were normalized by dividing the activity of each sensor by the global field power (GFP, i.e. standard deviation across sensors) at each time-point. For the current analysis, further temporal smoothing was applied by averaging the activity at each sensor in a 100-ms overlapping sliding window centered at a given time point in each trial. Additional information about data acquisition, pre-processing and task paradigm not pertaining to the current study is detailed elsewhere(Adibpour, Dubois and Dehaene-Lambertz, 2018) For infants, final dataset considered for further analyses included ~110 ± 60 trials (min= 38 , max = 246 trials) each for left and right faces, and ~ 32 ± 17 trials (min= 3, max=74 trials) for central faces condition. For adults, the final dataset included ~353 ± 33 (min= 255, max=363 trials) trials each for the left and right faces.

Trajectory in Principle Component (PC) Space.

For one example subject, 12s long segment of clean continuous EEG data containing 10 consecutive (left and right faces) trials were low-pass filtered using 100 ms overlapping sliding window. This segment of EEG data was normalized by dividing the activity at each

bioRxiv preprint doi: https://doi.org/10.1101/2021.03.07.434162; this version posted March 8, 2021. The copyright holder for this preprint (which was not certified by peer review) is the author/funder. All rights reserved. No reuse allowed without permission.

sensor by the instantaneous global field power. This standardized 128-dimensional time **x** channel matrix was transformed into three orthogonal components that explain a maximum amount of the variance (82% of total temporal variance was explained by first 3 components) using PCA decomposition from scikit-learn toolbox in python and the resulting PC coefficients were used to visualize 3-dimensional trajectory shown in Fig 1D.

Extracting ERP Templates.

For each condition (left, right and central) and for each cohort (infants and adults), we derived grand average ERP topography by averaging subject-specific ERP activity separately for each sensor across subjects (Fig 1B for infants, Fig S1A for adults). For infants, we identified 'P1 template' as grand-average topography in the range of ~225-275 ms post-stimulus for lateralized faces and in the range of ~125-175 ms post-stimulus for central faces. Similarly, 'P400-template' was derived as the average topography in the range of ~525-575 ms post-stimulus for both lateral and central faces (Fig S2 A). For adults, we identified 'P1 template' as the grand average topography in ~75-125 ms post-stimulus while 'P400 template' was identified as ~375-425 ms post-stimulus (Fig S2 B). These time-ranges were chosen by selecting a 50ms long time-window around the peak ERP response topography as inspected manually.

Measures of Trial-Variability

Measures of trial-variability (i.e. Flyby to known ERP Templates, Between-trial Variability and Within-trial Speed) were calculated as topographic dissimilarity using spatial correlation distance (1- Pearson correlation coefficient) as dispersion metric. Hence, absolute distances varied from 0 (absolute correlation) to 2 (no correlation). Correlation distance decouples the topographic patterns from their magnitudes; allowing us to focus on the relative spatial

bioRxiv preprint doi: https://doi.org/10.1101/2021.03.07.434162; this version posted March 8, 2021. The copyright holder for this preprint (which was not certified by peer review) is the author/funder. All rights reserved. No reuse allowed without permission.

patterns rather than their absolute magnitudes. Note that for our study, Correlation distance was mathematically equivalent to previously used Cosine dissimilarity measure since our data was reference averaged at each time-point (hence, mean across sensors equals to zero).

'Fly-by' to ERP Templates.

For each subject and for each condition, flyby distance from trial κ to a certain ERP template $\mathbf{X}$ at time τ was calculated as correlation distance,

$$\Delta(\kappa, \tau) = 1 - \Gamma(X, \Phi(\kappa, \tau))$$

Where, Γ is Pearson's correlation coefficient and $\Phi(\kappa, \tau)$ represents topography at trial κ and time τ. These single-trial distance time-series were further averaged across trials for each ERP template to obtain a single time-series per subject for P1 and P400 templates and for each condition (Fig 2 A).

'Fly-by' Latency and Distance. In the predefined time range for each ERP template, moments of closest 'flybys' to these templates were identified as the time-points when the distance Δ fell into the lowest 5 percentile of the overall distance distribution. Latency of these moments were used for the analyses of median and jitter in flyby latencies for each infant (**Fig 2B, Fig S3C,D**). The time-range to derive flybys was restricted to 150-350 ms for P1 template and 400-600 ms for P400 template in case of lateral faces. For central faces, 0-150 ms for P1 template and 350-550 ms for P400 template. For adults, the analysis was restricted to 0-150 ms for P1 and 150-500 ms for P400 template. These time-ranges were chosen based on the lowest flyby distance in the grand-average curves. Mean and S.D. of all single-trial flyby distances in these time-ranges were calculated for the comparison across subjects. (Fig 2C, Fig S3 E-H).

bioRxiv preprint doi: https://doi.org/10.1101/2021.03.07.434162; this version posted March 8, 2021. The copyright holder for this preprint (which was not certified by peer review) is the author/funder. All rights reserved. No reuse allowed without permission.

Between-Trial Variability

For each subject and for each condition, between-trial variability at time τ was calculated as the average of all pair-wise spatial correlation distances between all trial-pairs i and j;

$$\Delta(\tau) = \frac{1}{\binom{n}{2}} \sum_{ij} \left(1 - \Gamma(\Phi(i,\tau), \Phi(j,\tau))\right)$$

Where, n = number of trials, $\binom{n}{2}$ suggests all pair-wise combinations of trials, Γ is Pearson correlation coefficient and $\Phi(j,\tau)$ represents sensor topography at trial j and time-point τ.

One such absolute single-subject between-trial variability time-courses were derived per condition and further z-scored across time, to obtain relative between-trial variability. These z-scored time-series were further averaged in the previously defined time-range for P1 and P400-flybys to obtain relative between-trial variability around flybys (Fig 3, Fig S5).

Topography of Between-trial Variability Quenching.

If sensor χ has δ neighboring channels, Between-trial variability is calculated for this sensor at time τ as follows:

$$\Delta(\chi,\tau) = \frac{1}{\binom{n}{2}} \sum_{ij} \left(1 - \Gamma(\Phi\chi(i,\tau), \Phi\chi(j,\tau))\right)$$

Where, Γ is Pearson correlation coefficient; $(\Phi\chi(i,\tau)$ is δ + 1 dimensional activity vector at time τ and trial i, where each dimension represent neighbours of sensor χ (including itself). Neighbors of each channel were inferred from the channel-connectivity matrix estimated using find_ch_connectivity function of MNE-python. For each subject, instead of single global between-trial variability time-series, now we obtained one time-series

bioRxiv preprint doi: https://doi.org/10.1101/2021.03.07.434162; this version posted March 8, 2021. The copyright holder for this preprint (which was not certified by peer review) is the author/funder. All rights reserved. No reuse allowed without permission.

each for each sensor. This absolute sensor-level between-trial variability was further Z-scored across time to obtain relative variability for each sensor. These channel x time matrices for each subject were further averaged to obtain group-level between-trial variability topography. (Fig S4).

Within-Trial Speed

For each trial k, within-trial speed at time t was calculated as spatial correlation distance between topography at that time-point and the same at the consecutive time-point.

$$\Delta(\kappa, \tau) = 1 - \Gamma(\Phi(\kappa, \tau), \Phi(\kappa, \tau + 1))$$

Where, Γ is Pearson correlation coefficient and $\Phi(\kappa, \tau)$ represents sensor topography at trial κ and time-point τ. ***Overall*** absolute within-trial speed for each subject was obtained by first averaging speed time-courses across trials and then averaging the mean speed time-courses across time (Fig 4A).

Fly-by Triggered Speed Profiles. For each subject, moments of 'fly-by' to known ERP templates were identified as described above (trial-to-template distance falling in the lowest 5th percentile). Trial-speed segments at each occurrence of 'fly-by' were extracted as speed time-course from 400-ms before to 400-ms after 'fly-by'. Each of these 800-ms long speed time-courses were averaged to obtain a single speed profile per template (Fig 4B). These subject-specific absolute speed profiles were z-scored along the time dimension to obtain relative speed profiles around fly-by and further averaged to obtain group-average speed-profiles (Fig 4C , D; Fig S6A). To compare flyby triggered instantaneous speed across infants, peak speed (for P1 template) and lowest speed (for P400 template) were identified in the 100 ms time-window centered at 'flyby' moment (Fig 4 E-F, Fig S6 B-D).

bioRxiv preprint doi: https://doi.org/10.1101/2021.03.07.434162; this version posted March 8, 2021. The copyright holder for this preprint (which was not certified by peer review) is the author/funder. All rights reserved. No reuse allowed without permission.

Trial Speed Distribution. To obtain trial-speed distribution for each age-group per condition, all single-trial speed time-courses were concatenated along time and along subjects in that age-group to obtain one single speed distribution. Probability density was obtained by normalizing area under each bin to 1. Normalized bin-counts (density) were plotted on a log-log scale (Fig S6A, right).

Fitting power-law to the Trial Speed Distributions. We first temporally concatenated all the trials for each subject per each condition and age-group cohorts. This allowed us to reliably estimate the parameters for heavy-tailed distributions. We transformed the distribution of trial-speed into the standard normal distribution and finally fitted a least square regression line to the section of log-log plot achieved from the standard normal-distribution. We further repeated the procedure for each subject and obtained slopes and biases of the best-fit lines per subject and compared across the age-groups.

Statistics.

Potential linear age-trends were tested using one-tailed permutation test on Pearson Correlation Coefficient (number of permutation=1000). Significant reductions in variability time-courses were tested using one-sample t-test and correction for multiple comparison and temporal non-independence was applied using cluster based permutation test as implemented in MNE-python(Gramfort *et al.*, 2013). Group-level differences between paired groups of variables (variability in lateral vs central faces) were tested using nonparametric two-tailed Wilcoxon signed-rank tests (from Sci-py package). Group differences between 5-12 week old (first trimester) infants, 16-24 week old (second trimester) infants and adults were tested using non-parametric Kruskal-wallis test (Sci-py implementation), followed by post-hoc pair-wise comparisons using Mann-Whitney U test with Bonferroni correction (using scikit-posthocs package).

bioRxiv preprint doi: https://doi.org/10.1101/2021.03.07.434162; this version posted March 8, 2021. The copyright holder for this preprint (which was not certified by peer review) is the author/funder. All rights reserved. No reuse allowed without permission.

REFERENCES

Adibpour, P., Dubois, J. and Dehaene-Lambertz, G. (2018) 'Right but not left hemispheric discrimination of faces in infancy', *Nature Human Behaviour*, 2(1), pp. 67–79. doi: 10.1038/s41562-017-0249-4.

ALLEN, D., TYLER, C. W. and NORCIA, A. M. (1996) 'Development of grating acuity and contrast sensitivity in the central and peripheral visual field of the human infant', *Vision Research*, 36(13), pp. 1945–1953.

Arazi, A., Censor, N. and Dinstein, I. (2017) 'Neural variability quenching predicts individual perceptual abilities', *Journal of Neuroscience*, 37(1), pp. 97–109.

Bastos, A. M. *et al.* (2015) 'Visual areas exert feedforward and feedback influences through distinct frequency channels', *Neuron*, 85(2), pp. 390–401.

Berkes, P. *et al.* (2011) 'Spontaneous cortical activity reveals hallmarks of an optimal internal model of the environment', *Science*, 331(6013), pp. 83–87.

Braddick, O. and Atkinson, J. (2011) 'Development of human visual function', *Vision research*, 51(13), pp. 1588–1609.

Broday-Dvir, R. *et al.* (2018) 'Quenching of spontaneous fluctuations by attention in human visual cortex', *NeuroImage*, 171(November 2017), pp. 84–98. doi: 10.1016/j.neuroimage.2017.12.089.

La Camera, G., Fontanini, A. and Mazzucato, L. (2019) 'Cortical computations via metastable activity', *Current opinion in neurobiology*, 58, pp. 37–45.

Chaudhuri, R. *et al.* (2019) 'The intrinsic attractor manifold and population dynamics of a canonical cognitive circuit across waking and sleep', *Nature Neuroscience*, 22(9), pp. 1512–1520. doi: 10.1038/s41593-019-0460-x.

Chiron, C. *et al.* (1997) 'The right brain hemisphere is dominant in human infants.', *Brain:*

bioRxiv preprint doi: https://doi.org/10.1101/2021.03.07.434162; this version posted March 8, 2021. The copyright holder for this preprint (which was not certified by peer review) is the author/funder. All rights reserved. No reuse allowed without permission.

a journal of neurology, 120(6), pp. 1057–1065.

Churchland, M. M. *et al.* (2010) 'Stimulus onset quenches neural variability: a widespread cortical phenomenon', *Nature neuroscience*, 13(3), pp. 369–378.

Clawson, W. *et al.* (2019) 'Computing hubs in the hippocampus and cortex', *Science advances*, 5(6), p. eaax4843.

Conte, S. *et al.* (2020) 'Face-sensitive brain responses in the first year of life', *NeuroImage*, 211, p. 116602.

Dehaene-Lambertz, G. and Spelke, E. S. (2015) 'The Infancy of the Human Brain', *Neuron*, 88(1), pp. 93–109. doi: 10.1016/j.neuron.2015.09.026.

Dubois, J. *et al.* (2008) 'Microstructural correlates of infant functional development: example of the visual pathways', *Journal of Neuroscience*, 28(8), pp. 1943–1948.

Emberson, L. L., Richards, J. E. and Aslin, R. N. (2015) 'Top-down modulation in the infant brain: Learning-induced expectations rapidly affect the sensory cortex at 6 months', *Proceedings of the National Academy of Sciences*, 112(31), pp. 9585–9590.

Ezaki, T. *et al.* (2017) 'Energy landscape analysis of neuroimaging data', *Philosophical Transactions of the Royal Society A: Mathematical, Physical and Engineering Sciences*, 375(2096), p. 20160287.

Gramfort, A. *et al.* (2013) 'MEG and EEG data analysis with MNE-Python', *Frontiers in neuroscience*, 7, p. 267.

Gütig, R. and Sompolinsky, H. (2006) 'The tempotron: a neuron that learns spike timing–based decisions', *Nature neuroscience*, 9(3), pp. 420–428.

De Haan, M., Johnson, M. H. and Halit, H. (2003) 'Development of face-sensitive event-related potentials during infancy: a review', *International Journal of Psychophysiology*, 51(1), pp. 45–58.

bioRxiv preprint doi: https://doi.org/10.1101/2021.03.07.434162; this version posted March 8, 2021. The copyright holder for this preprint (which was not certified by peer review) is the author/funder. All rights reserved. No reuse allowed without permission.

He, B. J. (2013) 'Spontaneous and task-evoked brain activity negatively interact', *Journal of Neuroscience*, 33(11), pp. 4672–4682.

Hennequin, G. *et al.* (2018) 'The Dynamical Regime of Sensory Cortex: Stable Dynamics around a Single Stimulus-Tuned Attractor Account for Patterns of Noise Variability', *Neuron*, 98(4), pp. 846-860.e5. doi: 10.1016/j.neuron.2018.04.017.

Hensch, T. K. and Fagiolini, M. (2005) 'Excitatory–inhibitory balance and critical period plasticity in developing visual cortex', *Progress in brain research*, 147, pp. 115–124.

Hesselmann, G. *et al.* (2008) 'Spontaneous local variations in ongoing neural activity bias perceptual decisions', *Proceedings of the National Academy of Sciences*, 105(31), pp. 10984–10989.

Huk, A., Bonnen, K. and He, B. J. (2018) 'Beyond trial-based paradigms: Continuous behavior, ongoing neural activity, and natural stimuli', *Journal of Neuroscience*, 38(35), pp. 7551–7558.

Jasper, H. H. (1937) 'Electrical signs of cortical activity.', *Psychological Bulletin*, 34(7), p. 411.

Jung, T. *et al.* (2001) 'Analysis and visualization of single-trial event-related potentials', *Human brain mapping*, 14(3), pp. 166–185.

Kabdebon, C. and Dehaene-Lambertz, G. (2019) 'Symbolic labeling in 5-month-old human infants', *Proceedings of the National Academy of Sciences*, 116(12), pp. 5805–5810.

Kenet, T. *et al.* (2003) 'Spontaneously emerging cortical representations of visual attributes', *Nature*, 425(6961), pp. 954–956.

Kennedy, H. *et al.* (2007) 'Self-organization and pattern formation in primate cortical networks', in *Novartis Foundation Symposium*. Wiley Online Library, p. 178.

Kouider, S. *et al.* (2015) 'Neural dynamics of prediction and surprise in infants', *Nature*

bioRxiv preprint doi: https://doi.org/10.1101/2021.03.07.434162; this version posted March 8, 2021. The copyright holder for this preprint (which was not certified by peer review) is the author/funder. All rights reserved. No reuse allowed without permission.

Communications, 6, pp. 1–8. doi: 10.1038/ncomms9537.

Litwin-Kumar, A. and Doiron, B. (2012) 'Slow dynamics and high variability in balanced cortical networks with clustered connections', *Nature neuroscience*, 15(11), pp. 1498–1505.

Lombardo, D. *et al.* (2020) 'Modular slowing of resting-state dynamic Functional Connectivity as a marker of cognitive dysfunction induced by sleep deprivation', *bioRxiv*, p. 2020.01.17.910810. doi: 10.1101/2020.01.17.910810.

Luck, S. J. (2012) 'Event-related potentials.'

Ma, W. J. *et al.* (2006) 'Bayesian inference with probabilistic population codes', *Nature neuroscience*, 9(11), pp. 1432–1438.

Maass, W., Natschläger, T. and Markram, H. (2002) 'Real-time computing without stable states: A new framework for neural computation based on perturbations', *Neural computation*, 14(11), pp. 2531–2560.

Mazor, O. and Laurent, G. (2005) 'Transient dynamics versus fixed points in odor representations by locust antennal lobe projection neurons', *Neuron*, 48(4), pp. 661–673.

McIntosh, A. R., Kovacevic, N. and Itier, R. J. (2008) 'Increased brain signal variability accompanies lower behavioral variability in development', *PLoS Computational Biology*, 4(7). doi: 10.1371/journal.pcbi.1000106.

Michel, C. M. and Koenig, T. (2018) 'EEG microstates as a tool for studying the temporal dynamics of whole-brain neuronal networks: A review', *Neuroimage*, 180, pp. 577–593.

Naik, S. *et al.* (2017) 'Metastability in Senescence', *Trends in Cognitive Sciences*, 21(7), pp. 509–521. doi: 10.1016/j.tics.2017.04.007.

Palmigiano, A. *et al.* (2017) 'Flexible information routing by transient synchrony', *Nature Neuroscience*, 20(7), pp. 1014–1022. doi: 10.1038/nn.4569.

Pillai, A. S. and Jirsa, V. K. (2017) 'Symmetry breaking in space-time hierarchies shapes

bioRxiv preprint doi: https://doi.org/10.1101/2021.03.07.434162; this version posted March 8, 2021. The copyright holder for this preprint (which was not certified by peer review) is the author/funder. All rights reserved. No reuse allowed without permission.

brain dynamics and behavior', *Neuron*, 94(5), pp. 1010–1026.

Posner, M. I. and DiGirolamo, G. J. (2000) 'Cognitive neuroscience: Origins and promise.', *Psychological Bulletin*, 126(6), p. 873.

Rajan, K., Abbott, L. F. and Sompolinsky, H. (2010) 'Stimulus-dependent suppression of chaos in recurrent neural networks', *Physical Review E - Statistical, Nonlinear, and Soft Matter Physics*, 82(1). doi: 10.1103/PhysRevE.82.011903.

Sadaghiani, S., Hesselmann, G. and Kleinschmidt, A. (2009) 'Distributed and antagonistic contributions of ongoing activity fluctuations to auditory stimulus detection', *Journal of Neuroscience*, 29(42), pp. 13410–13417.

Schurger, A. *et al.* (2015) 'Cortical activity is more stable when sensory stimuli are consciously perceived', *Proceedings of the National Academy of Sciences*, 112(16), pp. E2083–E2092. doi: 10.1073/PNAS.1418730112.

Skarda, C. A. and Freeman, W. J. (1987) 'How brains make chaos in order to make sense of the world', *Behavioral and brain sciences*, 10(2), pp. 161–173.

Tenenbaum, J. B. *et al.* (2011) 'How to grow a mind: Statistics, structure, and abstraction', *science*, 331(6022), pp. 1279–1285.

Tsuda, I. (2009) 'Hypotheses on the functional roles of chaotic transitory dynamics', *Chaos: An Interdisciplinary Journal of Nonlinear Science*, 19(1), p. 15113.

Vahid, A. *et al.* (2020) 'Applying deep learning to single-trial EEG data provides evidence for complementary theories on action control', *Communications biology*, 3(1), pp. 1–11.

VanRullen, R. *et al.* (2011) 'Ongoing EEG phase as a trial-by-trial predictor of perceptual and attentional variability', *Frontiers in psychology*, 2, p. 60.

Verleger, R., Gasser, T. and Möcks, J. (1982) 'Correction of EOG artifacts in event-related potentials of the EEG: Aspects of reliability and validity', *Psychophysiology*,

bioRxiv preprint doi: https://doi.org/10.1101/2021.03.07.434162; this version posted March 8, 2021. The copyright holder for this preprint (which was not certified by peer review) is the author/funder. All rights reserved. No reuse allowed without permission.

19(4), pp. 472–480.

Wu, H. G. *et al.* (2014) 'Temporal structure of motor variability is dynamically regulated and predicts motor learning ability', *Nature neuroscience*, 17(2), pp. 312–321.

Zylberberg, A. *et al.* (2011) 'The human Turing machine: A neural framework for mental programs', *Trends in Cognitive Sciences*, 15(7), pp. 293–300. doi: 10.1016/j.tics.2011.05.007.

bioRxiv preprint doi: https://doi.org/10.1101/2021.03.07.434162; this version posted March 8, 2021. The copyright holder for this preprint (which was not certified by peer review) is the author/funder. All rights reserved. No reuse allowed without permission.

Figures for the manuscript

"Structured Modulations of Ongoing Variability by Task and Development"

Note: All faces presented as stimuli are replaced by gray squares in adherence to the Biorxiv privacy policy. The squares are representative of the relative position where originally the face stimuli appeared.

Figure 1

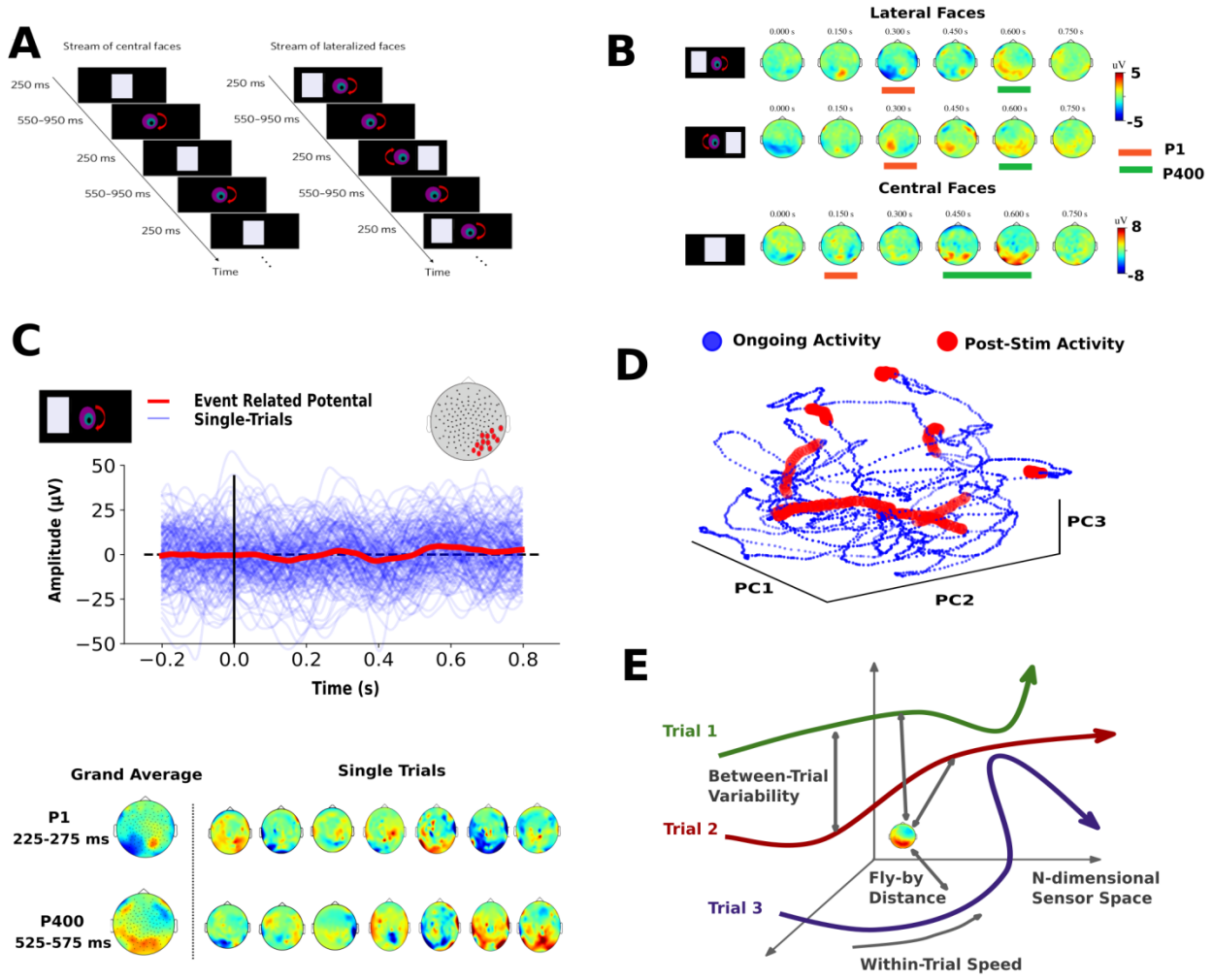

bioRxiv preprint doi: https://doi.org/10.1101/2021.03.07.434162; this version posted March 8, 2021. The copyright holder for this preprint (which was not certified by peer review) is the author/funder. All rights reserved. No reuse allowed without permission.

Figure 2

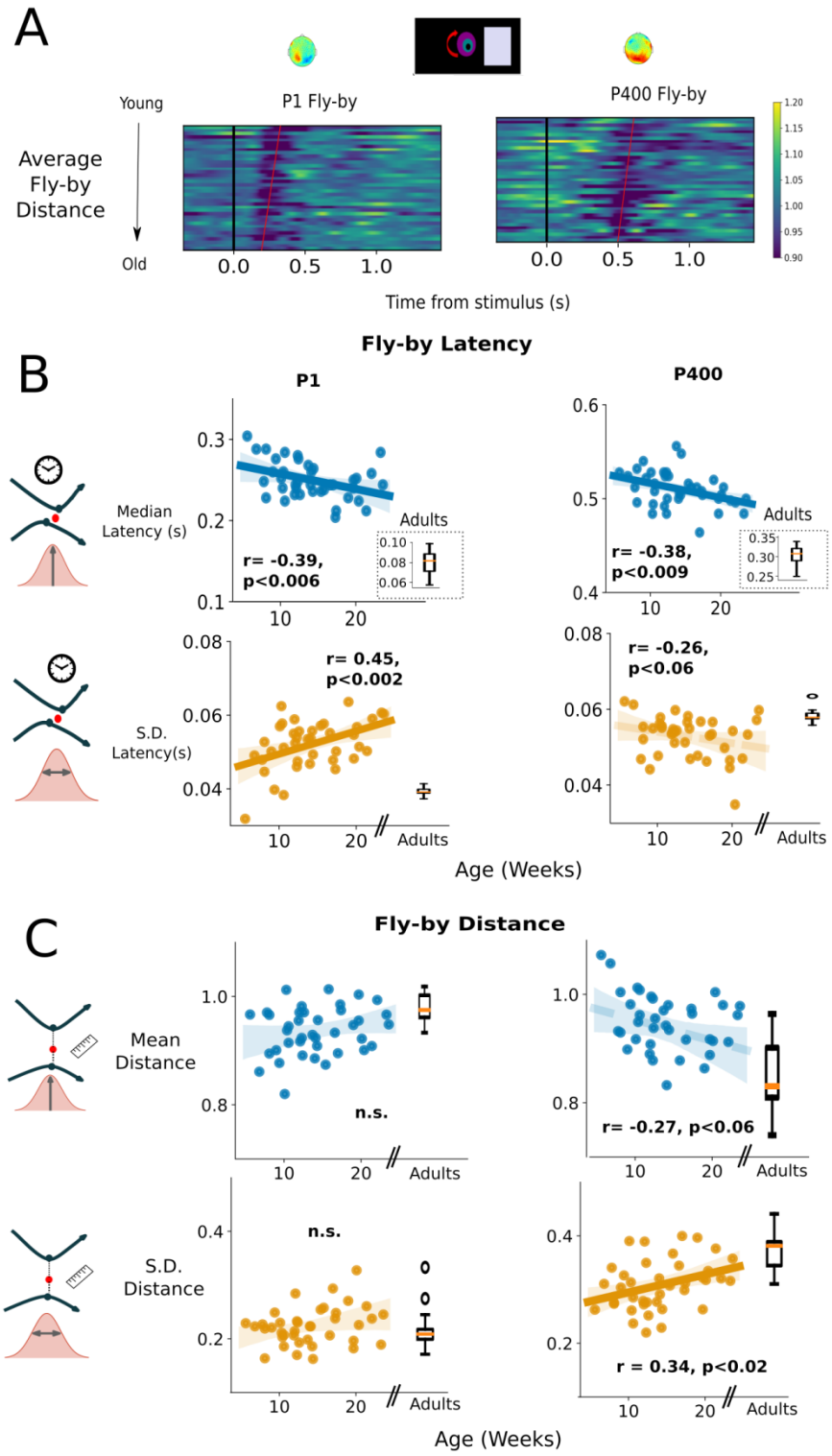

bioRxiv preprint doi: https://doi.org/10.1101/2021.03.07.434162; this version posted March 8, 2021. The copyright holder for this preprint (which was not certified by peer review) is the author/funder. All rights reserved. No reuse allowed without permission.

Figure 3

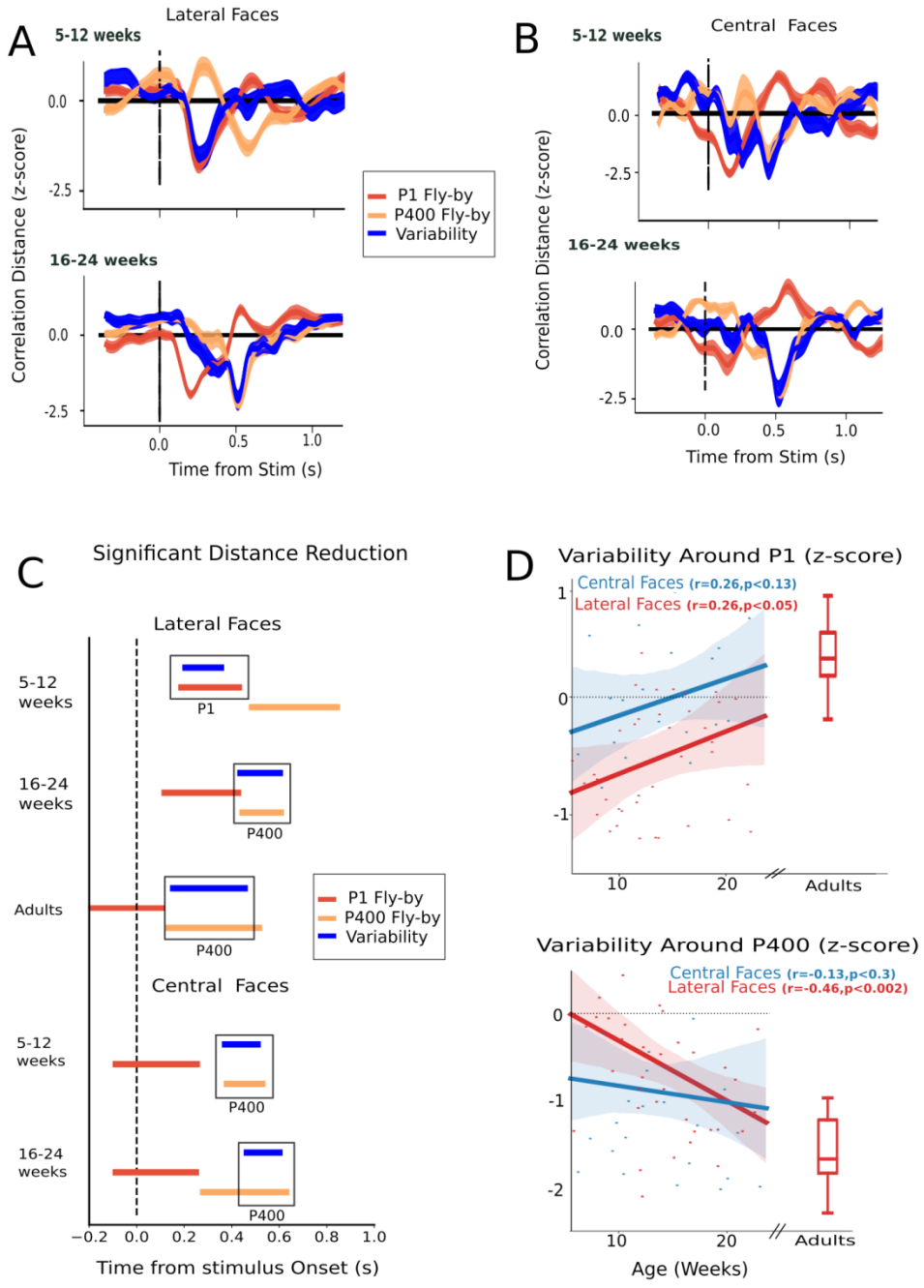

bioRxiv preprint doi: https://doi.org/10.1101/2021.03.07.434162; this version posted March 8, 2021. The copyright holder for this preprint (which was not certified by peer review) is the author/funder. All rights reserved. No reuse allowed without permission.

Figure 4